High-speed wave-mixing laser Doppler imaging, in vivo.

Michael Atlan, Michel Gross, Tania Vitalis, Armelle Rancillac, Jean Rossier,
Claude Boccara

High-speed wave-mixing laser Doppler imaging, in vivo.

M Atlan,[1] M Gross,[1] T Vitalis,[2] A Rancillac,[2] J Rossier,[2] and AC Boccara[3]

[1]Laboratoire Kastler-Brossel de l'École Normale Supérieure,
CNRS UMR 8552. Université Pierre et Marie Curie - Paris 6,
24 rue Lhomond 75231 Paris cedex 05. France.
[2]Laboratoire de Neurobiologie et Diversité Cellulaire de l'École
Supérieure de Physique et de Chimie Industrielles de la Ville de Paris,
CNRS UMR 7637. 10 rue Vauquelin 75231 Paris cedex 05. France.
[3]Laboratoire d'Optique de l'École Supérieure de Physique et de Chimie Industrielles de la Ville de Paris,
CNRS UPR 5, Université Pierre et Marie Curie - Paris 6,
10 rue Vauquelin 75231 Paris cedex 05. France.
(Dated: March 7, 2008)

An interferometric method for parallel optical spectroscopy in the kilohertz range is reported, as well as its experimental validation in the context of high speed laser Doppler imaging *in vivo*. The interferometric approach enables imaging in the low light conditions of a 2 kHz frame rate recording with a complementary metal-oxide semi-conductor (CMOS) camera. Observation of a mice cranium with near infrared ($\lambda = 785$ nm) laser light in reflection configuration is reported. Doppler spectral images allegedly sensitive to blood flow are measured at several optical frequency detunings sequentially, to shift the spectral range of analysis in the radiofrequency (RF) spectrum.

The low frequency part of the RF spectrum of visible and near infrared light is a witness of microvascular hemodynamics [1] and hence a subject of great interest for blood flow imaging applications. The observation and interpretation of RF broadening of a scattered laser light beam by a fluid in motion [2] has led to the development of laser Doppler velocimetry and imaging *in vivo* [3]. Other ways of imaging an optical contrast from microvascular flow include speckle contrast analysis [4–6]. Standard scanning laser Doppler instruments [7], based on time-domain measurements, provide spatial resolution at the expense of temporal resolution. Widefield, self-mixing light scattering laser Doppler techniques with a fast CMOS camera [8] provide an alternative to speckle contrast analysis to perform wide-field imaging of bioflow. But performance in terms of spatial, temporal, and velocity resolution, as well as sensitivity, is a major issue. The instrumental approach described in this Letter combines two methods designed for parallel laser Doppler imaging by means of interferometry with a separate reference beam [9, 10]. We report a substantial increase in temporal resolution with respect to heterodyne frequency-domain imaging [9] and the ability to explore the RF spectrum beyond the detector bandwidth, which is a limitation of the parallel Fourier-transform spectroscopy (FTS) scheme [10].

The experimental apparatus, sketched in Fig.1, is an optical interferometer designed for the collection of backscattered light from exposed mice cranial bone. Animal procedures were conducted in compliance with the European Communities Council directive 86-16-09/EEC. In total, three C57/Bl6 mice aged P50 to P55 were used. Anesthesia was achieved by injecting 85 mg/kg intraperitoneal of pentobarbital. Cranial skin and subcutaneous tissues were excised and cortical bones were preserved.
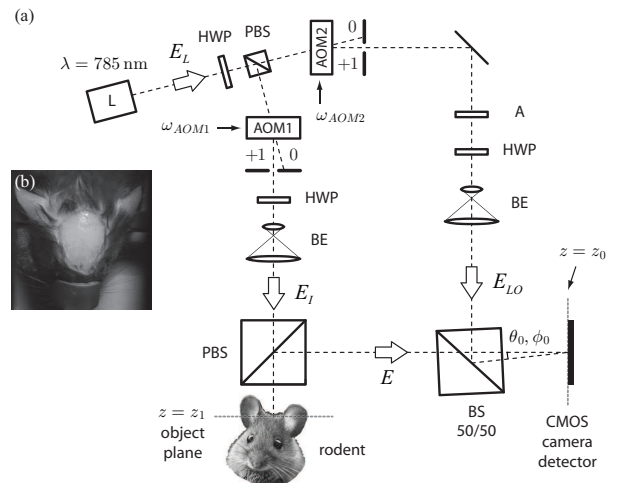

FIG. 1: (a) : Experimental scheme. Acronyms are defined in text. (b) White-light picture of the animal preparation.

Animals were positioned on a stereotaxic frame (World Precision Instruments) to ensure stability of the preparation. A continuous diode laser (L), 80 mW power, $\lambda = 785$ nm provides the main single mode laser beam (field E_L at optical frequency ω_L), polarized linearly. The beam is split by a polarizing beam splitter (PBS) into local oscillator (LO) and object arms. The power ratio between the LO (E_{LO} field) and the object arm (E_I field) is tuned by tilting the polarization angle of the main beam with a $\lambda/2$ waveplate (HWP) in front of the PBS. The beams optical frequencies are shifted independently by a pair of acousto-optic modulators (AOM 80 MHz, AA optoelectronic) driven with tunable signals from phaselocked RF generators at frequencies ω_{AOM_1} (object) and ω_{AOM_2} (LO). In the object arm, a PBS is used to shine

the preparation and collect the cross-polarized backscattered light component, to select photons which have undergone at least a few scattering events [11]. This approach is chosen to increase the weight of multiply scattered Doppler-shifted photons with respect to photons backscattered by the upper cranial bone layers. The incident light beam is expanded over $1 \times 1\,\mathrm{cm}^2$ and its polarization angle is tuned with a HWP to set the illumination power to ~ 20 mW (in compliance with FDA norms). In the reference arm, an attenuator (A) of optical density = 2, a HWP, and a beam expander (BE) are used to control the LO beam power, polarization angle, and to ensure a flat LO illumination of the detector. The backscattered field E is mixed with the LO field E_{LO} with a non polarizing beam splitter cube (BS). The LO beam polarization angle is adjusted to maximize fringe modulation depth. Temporal fluctuations of the interference pattern $I = |E + E_{\mathrm{LO}}|^2$ are measured by a CMOS camera (LaVision HSS 4, 10 bit (1024 counts) dynamic range, 1024×1024 pixels at $\omega_{\mathrm{S}} = 2.0$ kHz frame rate, pixel size $d = 17.5\ \mu m$, set at a distance $\Delta z = 61$ cm from the object plane. Backscattered photons account for $|E|^2 = 0.76$ digital count per pixel on average, and LO light fills most of the detector dynamic range : $|E_{\mathrm{LO}}|^2 = 379$ counts. A small angular tilt $\theta_0, \phi_0 \simeq 1°$ is made between both beams to create off-axis recording conditions and provoke spatial fringes in the interference pattern. Additionally, temporal modulation of these fringes is controlled by the optical frequency detuning $\Delta\omega_{\mathrm{AOM}} = \omega_{\mathrm{AOM}_2} - \omega_{\mathrm{AOM}_1}$.

Optical fields are described by scalar continuous variables. The dynamically scattered object field is :

$$E(x,y,z,t) = \mathcal{E}(x,y,z,t)e^{i\omega_{\mathrm{L}}t}e^{i\omega_{\mathrm{AOM}_1}t} \qquad (1)$$

where $\mathcal{E}$ is its complex envelope. The LO is a monochromatic plane wave :

$$E_{\mathrm{LO}}(x,y,z,t) = \mathcal{E}_{\mathrm{LO}}e^{i\omega_{\mathrm{L}}t}e^{i\omega_{\mathrm{AOM}_2}t}e^{i(k_{0x}x+k_{0y}y)} \qquad (2)$$

where $\mathcal{E}_{\mathrm{LO}}$ is the LO field complex envelope, which has no x,y,t dependencies. $k_{0x} \simeq 2\pi\theta_0/\lambda$, $k_{0y} \simeq 2\pi\phi_0/\lambda$ are the projections of the LO wave vector in the transverse (x,y) plane. The intensity $I(x,y,t)$ in the detector plane is :

$$
\begin{aligned}
I = {} & |\mathcal{E}(x,y,z_0,t)|^2 + |\mathcal{E}_{\mathrm{LO}}|^2 \\
& + \mathcal{E}(x,y,z_0,t)\mathcal{E}_{\mathrm{LO}}^* e^{-i(\Delta\omega_{\mathrm{AOM}}t+k_{0x}x+k_{0y}y)} \\
& + \mathcal{E}^*(x,y,z_0,t)\mathcal{E}_{\mathrm{LO}} e^{+i(\Delta\omega_{\mathrm{AOM}}t+k_{0x}x+k_{0y}y)}
\end{aligned} \qquad (3)
$$

where * denotes the complex conjugate. The two first terms of the right member of eq. 3 are the self beating (homodyne) contributions of E and E_{LO}. Our signal lies in the LO-object field cross-terms in equation 3. These terms are the heterodyne object field distribution $I_{+1}(x,y,t) = \mathcal{E}(x,y,z_0,t)\mathcal{E}_{\mathrm{LO}}^* e^{-i(\Delta\omega_{\mathrm{AOM}}t+k_{0x}x+k_{0y}y)}$ and its conjugate $I_{-1} = I_{+1}^*$ (dual image). The recorded field
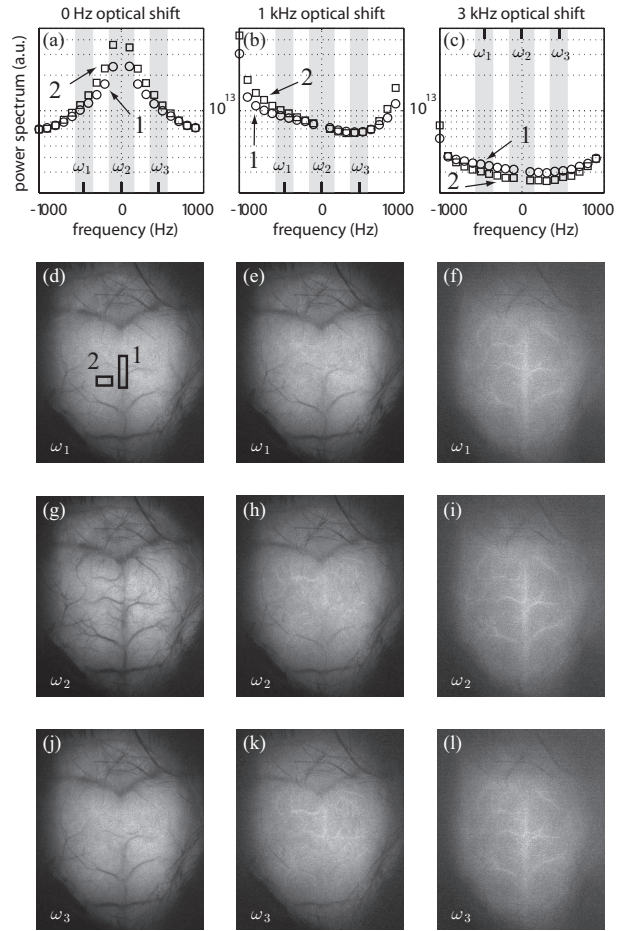

FIG. 2: Spectra (a to c) and image components of the cranium area (d to l), in log. scale. Spectra (circles and squares, respectively) are measured in the regions of interest 1 and 2, sketched on (d). Columns display results obtained at three optical frequency shifts : $\Delta\omega_{\mathrm{AOM}} = 0$ Hz (a, d, g, j), $\Delta\omega_{\mathrm{AOM}} = 1000$ Hz (b, e, h, k), $\Delta\omega_{\mathrm{AOM}} = 3000$ Hz (c, f, i, l). Rows show images of three Fourier sidebands of the spectrum (displayed in gray on figs. a, b, c) : $\omega_1 = -450$ Hz (d, e, f), $\omega_2 = 0$ Hz (g, h, i), $\omega_3 = +450$ Hz (j, k, l).

interference pattern $I(x,y,t)$ measured in the detector plane $(z = z_0)$ is then back-propagated numerically at $z = z_1$ with a Fresnel transform for holographic image reconstruction :

$$H(x,y,t) = I(x,y,t) * \frac{1}{i\lambda\Delta z}e^{ik\Delta z}e^{i\frac{k}{2\Delta z}(x^2+y^2)} \qquad (4)$$

where $k = 2\pi/\lambda$, $\Delta z = z_1 - z_0$ (= 61 cm), and $*$ is the convolution product for variables x, y. Because of off-axis wave mixing, the Fresnel transform decouples spatially the heterodyne terms of eq.3, yielding the ± 1 order images $H_{\pm 1}$, from the self-mixing terms, yielding the 0 order image H_0. Hence we can filter-off spatially [10, 12] the -1 and 0 order images from H and isolate the distribution of the object field envelope in the object plane
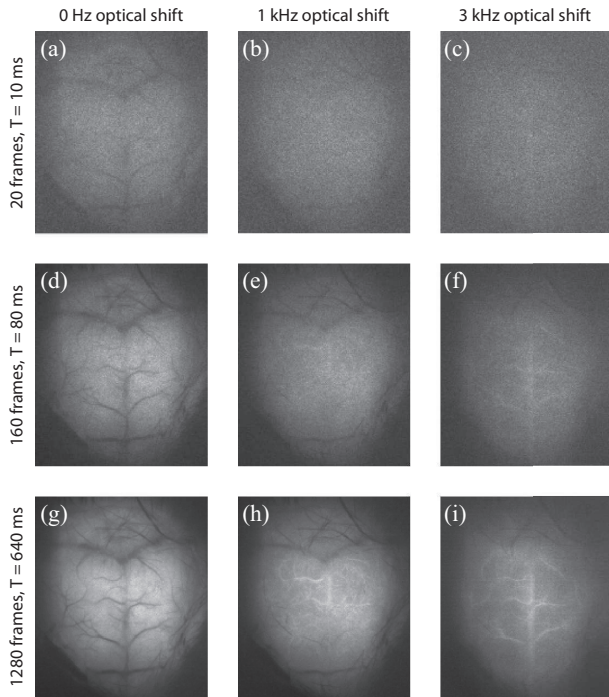
FIG. 3: Spectral images in log. scale averaged in the +100 Hz to +500 Hz frequency band at three different optical shifts : $\Delta\omega_{\text{AOM}} = 0\,\text{Hz}$ (a, d, g), $\Delta\omega_{\text{AOM}} = 1000\,\text{Hz}$ (b, e, h), $\Delta\omega_{\text{AOM}} = 3000\,\text{Hz}$ (c, f, i). Temporal resolution vary from 10 ms (a, b, c) to 640 ms (g, h, i).

$(z = z_1)$, at time t :

$$H_{+1}(x,y,t) \sim \mathcal{E}(x - x_0, y - y_0, z_1, t)\mathrm{e}^{-i\Delta\omega_{\text{AOM}}t} \quad (5)$$

where $x_0 \propto \theta_0$ and $y_0 \propto \phi_0$. A temporal Fourier transform of the time-resolved H_{+1} quantity yields :

$$\widetilde{H}_{+1}(x,y,\omega) \sim \widetilde{\mathcal{E}}(x - x_0, y - y_0, z_1, \omega - \Delta\omega_{\text{AOM}}) \quad (6)$$

Images of the object field envelope $S(x,y,\omega) = |\widetilde{H}_{+1}(x,y,\omega)|^2$, represented in Figs. 2(d, g, j) and 3(a, d, g, j) in arbitrary logarithmic units, are then computed from a 20-point discrete Fourier transform averaged on 1280 consecutive data frames (acquired in 640 ms). The 2 kHz image acquisition rate sets a spectral range centered on DC and bounded by the Nyquist frequencies $\pm$ 1 kHz. This spectral range of analysis can be translated by heterodyning, achieved by tuning $\Delta\omega_{\text{AOM}}$.

Three 200 Hz-wide frequency bands of the FTS spectral range, centered on $\omega_1 = $ -450 Hz, $\omega_2 = 0$ Hz, and $\omega_3 = +450$ Hz, are displayed in figs. 2(d to l), for three different optical shifts $\Delta\omega_{\text{AOM}} = 0$ Hz, 1 kHz, 3 kHz. The contrast inversion between vessels and the surrounding matrix for increasing values of $\Delta\omega_{\text{AOM}}$ is attesting of the Doppler frequency signature of blood flow [9]. $S(x,y,\omega)$ **is** averaged spatially in two nearby regions of interest between which the inversion is observed. These regions, noted '1' and '2', are shown on fig.2(d). Spectra of the

two regions of interest are displayed in figs.2(a, b, c), for $\Delta\omega_{\text{AOM}} = 0$ Hz, 1 kHz, 3 kHz respectively. Under the assumption that the scattering properties are comparable in both regions, region 1 is the site of a larger bioflow than region 2 since dispersion is broader. The spectral component at null frequency (not represented) is mainly sensitive to DC noise. Furthermore, a stray signal increase is observed around the cutoff frequencies $\pm$ 1 kHz in figs.2(b, c). We interpret these aliases as a consequence of the $\text{sinc}^2(\pi\omega/\omega_{\text{S}})$-shaped response function of discrete FTS, folded in the spectral range bounded by $\pm\omega_{\text{S}}/2$. Fig. 3 displays the cranial image signal in the frequency band from +100 Hz to +500 Hz for $\Delta\omega_{\text{AOM}} = 0$ Hz, 1 kHz, 3 kHz (columns), and averaged in time from 10 ms to 640 ms (rows). In comparison, the acquisition time needed to measure such contrasts with the ref. [9] approach is more than two orders of magnitude higher. Moreover, the method presented here benefits from optical heterodyning, which allows to shift the band of analysis of wave-mixing FTS with a high speed camera [10] in a region of interest of the RF spectrum to assess the Doppler signatures of bioflows.

In conclusion, we have proposed a method for high speed, wide-field imaging of the radiofrequency spectrum of near infrared laser light, based on an interferometer with separate local oscillator and illumination beams. Fourier transform spectroscopy of the recorded temporal field fluctuations sets the spectral range and resolution, while optical frequency detuning of the local oscillator with respect to the illumination field allows to shift this spectral range away from DC. The method is validated by a laser Doppler measurement of multiply scattered light on a mouse model, *in vivo*. Parallel imaging of 20-point spectral images in 2 kHz windows with a temporal resolution down to 10 milliseconds is reported, which opens the way to time-resolved functional imaging of microflows, in vivo.

Corresponding author : atlan@lkb.ens.fr

[1] Robert Lohwasser and Gerald Soelkner. Experimental and theoretical laser-doppler frequency spectra of a tissuelike model of a human head with capillaries. *Appl. Opt.*, 38(10):2128–2137, 1999.

[2] Y. Yeh and H. Z. Cummins. Localized fluid flow measurements with an he-ne laser spectrometer. *Appl. Phys. Lett.*, 4:176–179, 1964.

[3] MD Stern, DL Lappe, PD Bowen, JE Chimosky, GA Holloway, HR Keiser, and RL Bowman. Continuous measurement of tissue blood flow by laser-doppler spectroscopy. *American journal of physiology*, 232(4):H441–H448, 1977.

[4] A. F. Fercher and J. D. Briers. Flow visualisation

by means of single-exposure speckle photography. *Opt. Commun.*, 37:326–330, 1981.

[5] J. D. Briers and Sian Webster. Laser speckle contrast analysis (lasca): a nonscanning, full-field technique for monitoring capillary blood flow. *Journal of Biomedical Optics*, 1(2):174–179, 1996.

[6] A. Dunn, H. Bolay, M. A. Moskowitz, and D. A. Boas. Dynamic imaging of cerebral blood flow using laser speckle. *Jounal of Cerebral Blood Flow and Metabolism*, 21(3):195–201, 2001.

[7] TJH Essex and PO Byrne. A laser doppler scanner for imaging blood flow in skin. *J Biomed Eng*, 13(3):189–194, 1991.

[8] A. Serov, W. Steenbergen, and F. de Mul. Laser doppler perfusion imaging with complementary metal oxide semiconductor image sensor. *Optics Letters*, 27:300–302, 2002.

[9] M. Atlan, M. Gross, T. Vitalis, A. Rancillac, B. C. Forget, and A. K. Dunn. Frequency-domain, wide-field laser doppler in vivo imaging. *Optics Letters*, 31(18):2762–2764, 2006.

[10] Michael Atlan and Michel Gross. Wide-field fourier transform spectral imaging. *Applied Physics Letters*, 91(11):113510, 2007.

[11] JM Schmitt, AH Gandjbakhche, and RF Bonner. Use of polarized light to discriminate short-path photons in a multiply scattering medium. *Appl. Opt*, 31(30):6535, 1992.

[12] Etienne Cuche, Pierre Marquet, and Christian Depeursinge. Spatial filtering for zero-order and twin-image elimination in digital off-axis holography. *Applied Optics*, 39(23):4070, 2000.